	Document:	Handbook	
	Author:	FEMTIKA	Version: 1
			Date: 29/6/2022




Project Acronym:	FEMTOSURF
Project Full Title:	Functional surface treatments using ultra-short pulse laser system
Grant Agreement:	825512
Project Duration:	1 January 2019 – 30 June 2022

## Handbook

Lead Beneficiary:	Femtika
Due Date:	Month 42
Document Status:	Final
Dissemination Level:	Public
File Name:	FemtoSurf Handbook

## FEMTOSURF Consortium

  <small>PHOTONICS PUBLIC PRIVATE PARTNERSHIP</small>
<p><b>This project received funding from the European Union's Horizon 2020 Research and Innovation programme under Grant Agreement No. 825512.</b></p> <p><b>This project is funded by one of the call under the Photonics Public Private Partnership (PPP) (<a href="http://www.photonics21.org">www.photonics21.org</a>)</b></p>

	Document:	Handbook		
	Author:	FEMTIKA	Version:	1
			Date:	29/6/2022

Participant No	Participant organization name	Country
1 (Coordinator)	Femtika	Lithuania
2 Partner	Amphos	Germany
3 Partner	FORTH	Greece
4 Partner	SUPSI	Switzerland
5 Partner	ROLLA	Switzerland
6 Partner	Aerea	Italy
7 Partner	MTC	United Kingdom
8 Partner	Heliotis	Switzerland
9 Partner	Straumann	Switzerland
10 Partner	Ramteid	Germany

### Authors List


Leading Author (Editor)			
Surname	First Name	Beneficiary	Contact email
Nemickas	Gedvinas	Femtika	Gedvinas.nemickas@femtika.com

### Reviewers List

List of Reviewers (in alphabetic order)			
Surname	First Name	Beneficiary	Contact email
Zemaitis	Arnas	Femtika	arnas.zemaitis@femtika.com


### Revision Control

Version	Status	Modifications made by
0.1	Initial Draft	11 January 2022
0.3	Final improvements	25 May 2022
1	Publication in webpage	29 June 2022

	Document:	Handbook	
	Author:	FEMTIKA	Version: 1
			Date: 29/6/2022

# Contents


Contents .....	3
1 Introduction.....	5
1.1 FemtoSurf application areas.....	12
2 Laser surfaces processing experimentation .....	14
2.1 Laser parameters effect on materials and alloys, wettability, and topography testing.....	14
2.2 Heat treatment effect on wettability.....	21
3 High power laser development.....	24
3.1 Design of Pumping scheme.....	24
5 FemtoSurf machine .....	27
6 Confidentiality .....	30

	Document:	Handbook		
	Author:	FEMTIKA	Version:	1
			Date:	29/6/2022

The present document is a Handbook of the FemtoSurf project (Grant Agreement No.: 825512), funded by the European Union's Horizon 2020 Research and Innovation program (H2020).

The FemtoSurf handbook for designing and managing FemtoSurf technology. This book concerns the overall FemtoSurf approach for configuring and controlling industrial-grade kW-level ultra-short laser machine.

The following document made use of the HORIZON 2020 FAIR DATA MANAGEMENT PLAN TEMPLATE and was written with reference to the Guidelines to FAIR (Findable, Accessible, Interoperable, and Reusable) data management in Horizon 2020.

	Document:	Handbook		
	Author:	FEMTIKA	Version:	1
			Date:	29/6/2022

# 1 Introduction

Femtosecond laser micromachining has emerged in recent years as a new technique for surface micro/nano structure fabrication. One of the key advances in the field is capability to produce high fidelity micro- and nano-features on metal surfaces (“ripples”). It is applicable to virtually any material and is performed in scalable, one-step fabrication process. In the past, much research on laser micromachining was carried out to understand the complex ablation mechanism, whereas recent works are mostly concerned with the fabrication of surface structures because of their numerous possible applications. It should be noted that the resulting surface morphology and subsequent properties heavily depend on the pulse duration of the laser with femtosecond (fs) pulses showing the greatest potential.

Surface micro/nano structuring creates many different structures on various materials. There is a huge variety of laser inscribed structures, whereas for laser-irradiated structures only a few types of structures are reported. The classification of surface structures is shown in Figure 1, along with a timeline for the milestones of laser micro/nanostructuring and other related works.

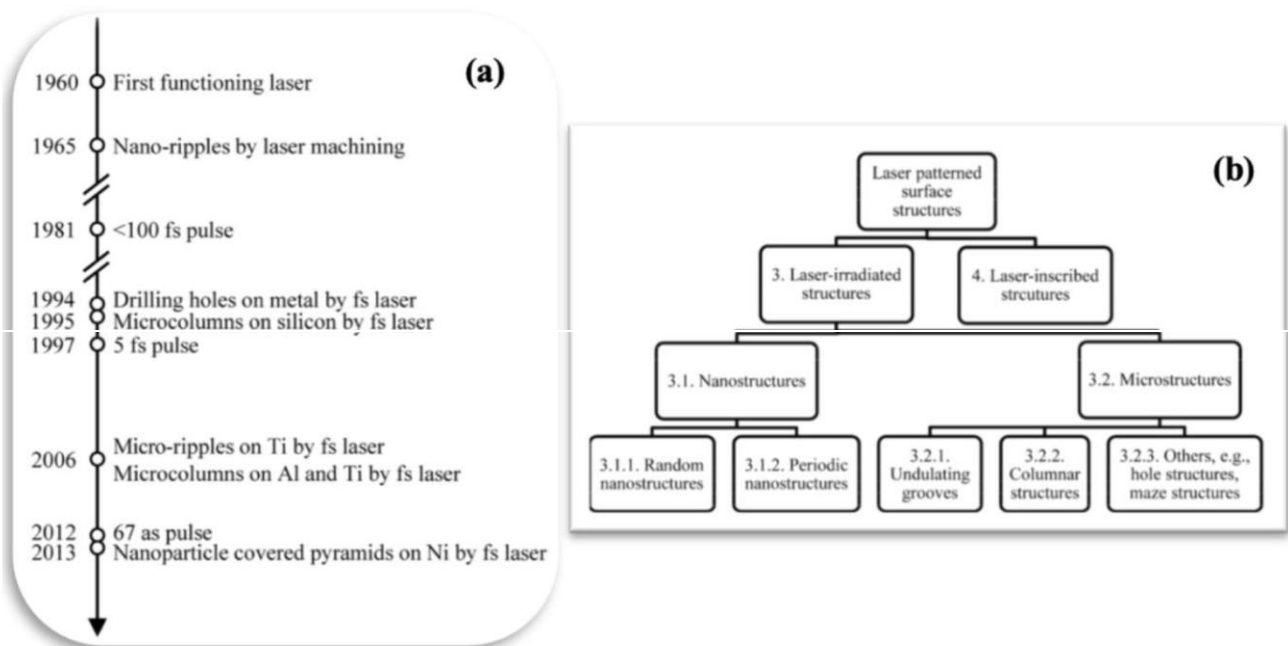



Figure 1: (a) Timeline of fs laser micro/nanostructuring and other related works and (b) classification of laser patterned surface structures.

Interestingly, direct laser machining can create structures on the nanometer scale, i.e. a lot smaller than the wavelength used to make them. Nanostructures can appear alone, or they can be associated with microstructures forming so-called hierarchical surface ripples. The two main types of nanostructures are random nanostructures and periodic nanostructures. Laser-induced periodic surface structures (LIPSS) were first observed in 1965. LIPSS are periodic nanostructures constituted of alternate crests and troughs. LIPSS produced by long-pulsed lasers has smooth features, whereas LIPSS densely covered with nanostructures. In consideration of periodicity, two distinct types of fs-LIPSS or FLIPSS are observed. The low-spatial-frequency LIPSS (LSFL) have a periodicity close to the laser wavelength. LSFL are

	Document:	Handbook		
	Author:	FEMTIKA	Version:	1
			Date:	29/6/2022

perpendicular to the polarization of the incident laser beam. It means that the grating vector of the LIPSS is parallel to the electric field polarization vector of the laser beam. The orientation of the high-spatial-frequency LIPSS (HSFL) that has a periodicity much smaller than the laser wavelength can be parallel or perpendicular to the beam polarization. Due to challenges faced in FemtoSurf the FLIPSS is deemed superior in the light of the project.

Researchers studied the effect of fs-laser irradiation process parameters (fluence and scanning speed) on the hydrophobicity of the resulting micro/nano-patterned morphologies on stainless steel. Depending on the laser parameters, four distinctly different nanopatterns were produced, namely nanorippled, parabolic-pillared, elongated sinusoidal-pillared, and triple roughness nano-structures, as shown next in Figure 2. Furthermore, Figure 2 shows several patterns manufactured in this study by varying the laser power between 5 and 1700 mW (fluence: 1.5-480 J/cm<sup>2</sup>) and scanning speed from 250 to 1850  $\mu$  m/s. In Figure 2, colored borders of each image show the ranges of laser power and scanning speed, which when used they generate the specific type of nano/microstructure. Thus, Figure 2 clearly indicates that lower laser fluence requires a higher number of laser pulses per spot to form a similar structure that can be formed by higher laser fluence. Decreasing the scanning speed corresponds to a higher number of laser pulses to create the micro-pattern. Therefore, the effects of increasing the laser fluence and decreasing the scanning speed are equivalent as both increase the diameter and height of pillars.

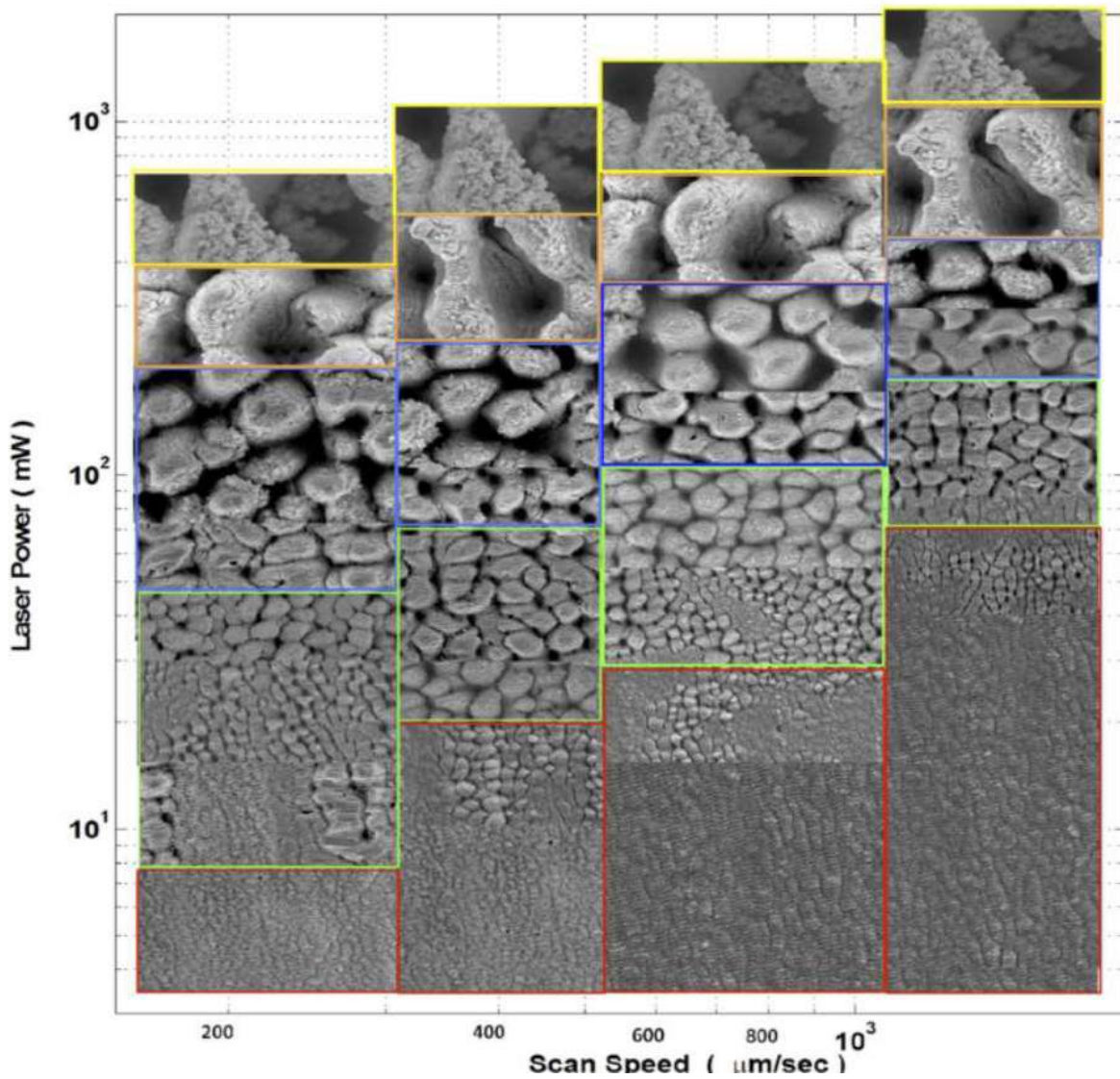


Figure 2: Formation of four patterns on stainless steel at various laser power and scanning speeds.

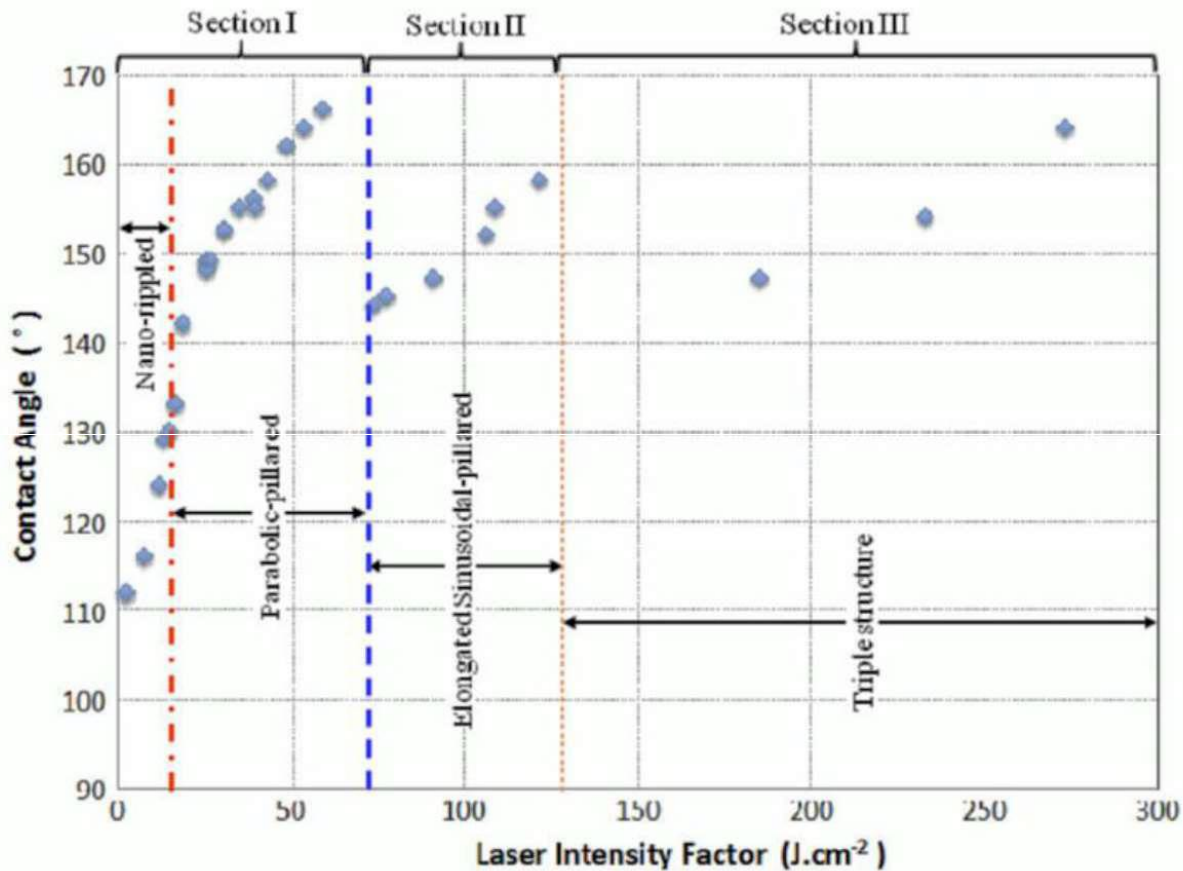


Figure 3: The Cassie-Baxter contact angle of various samples in the four distinctly different nano/micro-patterns on stainless steel as a function of the LIF parameter.

Next, the interaction of high-intensity fs-laser pulses with an example of steel alloy, has shown that ultrashort laser pulses are suitable for high-precision micromachining of this metal. Moreover, nearly no heat affected zone was observed in the neighboring of the laser processed microstructures and, in the case of the sintered hard metal, no decomposition and segregation due to the fs-laser interaction were detected. The femtosecond laser system permits material machining using the focusing technique, where the average wavelength of the fs-laser system is 775 nm, its maximum pulse energy 1 mJ, the pulse duration 150 fs and the constant pulse repetition rate 1 kHz. Layer by layer ablation is realized for producing 3D-microstructures, where the actual procedure is shown schematically in the following Figure 4. After constructing the desired 3D structure using CAD builder, a special converter software slices the structure into a stack of layers. Thereby, the layer thickness depends on the ablated depth per laser pulse, which is related to the material and the laser parameters and has to be determined in preparatory investigations. In the final step the computer program for controlling the sample motion and the laser, as well as the optical system in each layer is created. To avoid preferential directions each subsequent layer was machined with the laser beam moving direction perpendicular to the preceding one. The entire microstructure is thus produced by using layer-by-layer ablation. The ablation threshold and absorption coefficient were found 0.23 (J/cm²). Such functionality will be seamlessly included in the final workstation created during FemtoSurf.



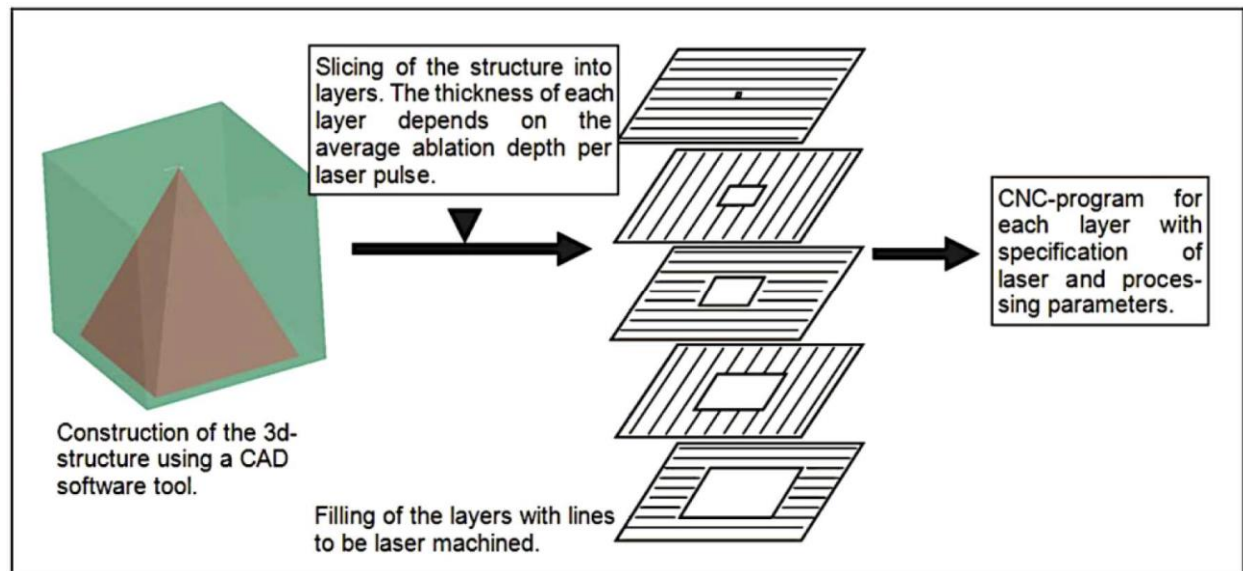



Figure 4: Schematic of the preparatory steps necessary for 3D micromachining. The 3d-structures were produced by using layer by layer ablation. The focal plane will be adjusted after the ablation of one layer.

According to the goals of FemtoSurf, produced surfaces should exhibit hydrophilic or hydrophobic properties. It was shown to be achievable with laser surface structuring. The Cassie-Baxter contact angle of the various samples is plotted versus the LIF parameter for the four distinct structures in the following Figure 5; as a final note, Figure 5, presents several SEM images of nano- patterns in each of the three sections of Figure 2, in increasing order of the LIF parameter with the contact angle also shown. Indeed, the fabrication of superhydrophobic surfaces induced by fs laser is a research hotspot nowadays. A simple and easily-controlled method for fabricating stainless steel-based superhydrophobic surfaces was presented. The method consists of micro-structuring stainless steel surfaces by irradiating samples with fs laser pulses and silanizing the surfaces. By low laser fluence, fabricated typical laser-induced periodic surface structures (LIPSS) on the submicron level. The apparent contact angle (CA) on the surface is  $150.3^\circ$ . With laser fluence increasing, they fabricated periodic ripples and periodic cone-shaped spikes on the micron scale, both covered with LIPSS. The stainless steel-based surfaces with micro and submicron double-scale structure have higher apparent CAs. On the surface of double-scale structure, the maximal apparent CA is  $166.3^\circ$  and at the same time, the sliding angle (SA) is  $4.2^\circ$  (Figure 7). The lotus leaf-like surface with double-scale structures is more easily to become superhydrophobic. The fraction of air between the water droplet and the double-scale surface is large, which is the important reason of super-hydrophobicity of the surface. It is important to note that such great results are a lot harder to achieve using longer pulses.

	Document:	Handbook		
	Author:	FEMTIKA	Version:	1
			Date:	29/6/2022

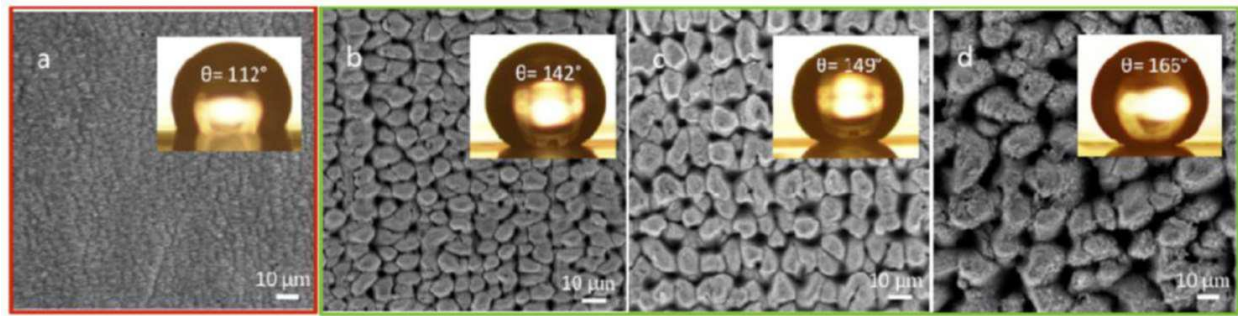



Figure 5: SEM images of nano-patterns on stainless steel (nano-rippled pattern, parabolic-pillared patterns) in increasing order of the LIF parameter with the contact angle also shown (a). LIF of 2.2 J/cm<sup>2</sup>, fluence of 1.5 J/cm<sup>2</sup> and scanning speed of 250 μm/s, (b) LIF of 18.65 J/cm<sup>2</sup>, fluence of 16 J/cm<sup>2</sup>, and scanning speed of 460 μm/s, (c) LIF of 25.16 J/cm<sup>2</sup>, fluence of 19.8 J/cm<sup>2</sup> and scanning speed of 370 μm/s, (d) LIF of 59.17 J/cm<sup>2</sup>, fluence of 38.2 J/cm<sup>2</sup> and scanning speed of 250 μm/s.

Experimental aspects of fs-Laser Material Processing are discussed. From the experimental viewpoint, the laser light is focused into the sample using microscope objectives with different numerical apertures (NAs), as shown in Figure 6 below. Alternatively, depending on the desired size of the features, lenses with larger focal distances can be used. Hence, as illustrated in the following Figure 6, a specific pattern is produced by either x-y sweeping the laser beam on the sample, which is kept fixed, with the aid of galvanometric mirrors (Figure 6a), or by using a three-dimensional (x-y-z) stage to translate the sample in respect to the fixed focusing lens (Figure 6b). In the first case (Figure 6a), the movement in the z-axis is achieved by an additional translation stage. The choice of which approach should be used depends on experimental details, such as processing time and area, laser repetition rate, etc. The movement of the sample or laser beam deflection is computer controlled, which defines not only the processing pattern on the sample but also the material processing speed, which is directly related to the number of pulses per laser spot for a given laser repetition rate. In order to visualize the material processing in real time, usually a CCD camera is coupled to the experimental setup.

Other experimental setups that include interference and diffraction processes have also been developed, allowing the fabrication of complex microstructures without the need of scanning the laser beam or translating the sample. Diffractive optical elements (DOEs), such as diffractive beam splitters play an important role in the multifocal micromachining and in the fabrication of periodic microstructures. The basic idea behind the use of DOEs is to produce multiple laser beams that are later focused at different angles, producing an interference pattern. Such modulation in the laser intensity is then transferred to the structure micromachined in the sample. All of these possibilities are considered in FemtoSurf.

	Document:	Handbook		
	Author:	FEMTIKA	Version:	1
			Date:	29/6/2022

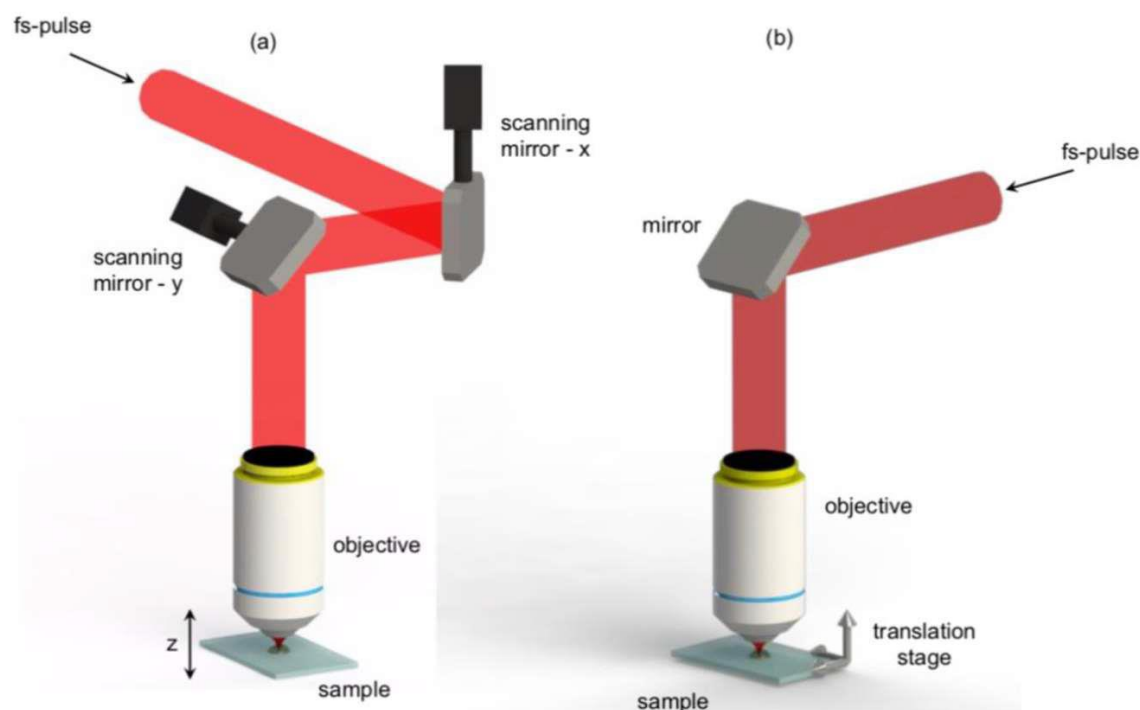



Figure 6: Schematic diagram of the experimental setup for laser processing of materials using (a) laser beam scanning mirror for beam deflection and (b) x-y-z translation stage for the sample.

Finally, one must not forget the importance of surface chemistry when considering hydrophobic and hydrophilic properties. Only with correct blend of both chemistry and topography effects commanded by FemtoSurf goals can be achieved. Thus, possible chemical treatment of laser structured surfaces must be considered. There are numerous examples of such functionalization in the literature. 316L stainless steel (SS) is one of the most widely used materials of construction. For example, a COOH-terminated alkanethiol (MUA) SAM was successfully formed on a 316L stainless steel surface using an electrochemical method. The stability of the monolayer was assessed by PMIRRAS, CA, and EIS. XPS demonstrated that the SAM was attached to the stainless steel surface through the MUA sulfur atom, although results also evidenced that some MUA molecules bound to the surface through both the thiol and the carboxylate group, exposing the hydrophobic alkane chain to the surface's exterior. The formed SAM was reasonably stable in a corrosive environment over a period of several days, and also withstood the exposure to fluid shear simulating blood circulation. Furthermore, the SAM also showed a substantial thermal stability at elevated temperatures. Therefore, such approach can be considered applicable to FemtoSurf samples, especially keeping in mind scalability and simplicity of such chemical post processing.

	Document:	Handbook		
	Author:	FEMTIKA	Version:	1
			Date:	29/6/2022

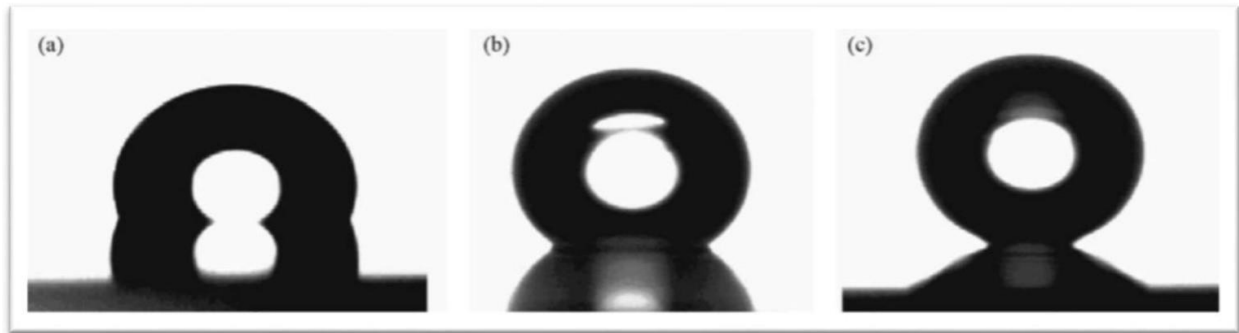


Figure 7: Photographs of water droplets on flat (a) LIPSS (b) and double-scale structure (c) AISI 316L type austenitic stainless steel-based surfaces after silanization.

### 1.1 FemtoSurf application areas

While the capabilities of laser surface patterning are highly promising, each application requires special attention to scales of surface features involved (figure 8). For instance, lubricants play an enormous role in modern tool manufacturing, reducing the wear of industrial tools and making the whole process smooth. However, sometimes getting lubricant to required places can be problematic or impossible. Ultrafast laser treatment of surfaces will address this issue in two ways. First, patterns can be created in order to guide lubricant to specific places of the machining setup. Second, friction can be reduced by special surface features in the operations where lubricant cannot be used due to adverse conditions of the process (for instance ultra-high temperature). As FemtoSurf is dedicated to metal surfaces it has synergy with the manufacturing sector where metal is a prevalent material of choice for its durability, property kept by the fabrication techniques applied in FemtoSurf.

FemtoSurf will also bring new solutions to the aerospace industry. Wear and contamination of aviation components operating under constant stress is a major issue. It requires constant cleaning/restoration operations that are complex and costly. Furthermore, spacecrafts operating beyond Earth's atmosphere cannot be reached for regular maintenance. Thus their operational wear or contamination should be minimized directly enhancing their lifespan. The surface treatment developed in FemtoSurf will remedy these problems by covering airplane or spacecraft components in surface patterns enhancing their self-cleaning properties and reducing the overall friction between components under heavy load enhancing their lifespan. It is important to note that due to the nature of light-matter interaction at fs time-scale any metal can be processed this way, including exotic alloys used in the aerospace industry. Fouling is a massive issue in all seafaring vessels. It results in increased drag and fuel consumption, raising both operational costs and the carbon footprint of ships. While hulls of ships can be to some extent covered with special anti-fouling coatings, propellers, operating in constant motion, cannot. For this reason, propeller cleaning becomes the only solution, further increasing operational costs, as sometimes it must be done in the intervals as small as two weeks. The anti-fouling surface structures on ship propellers will be implemented using fs laser surface patterning. It will lead to a massive decrease in fuel consumption and maintenance of ships, directly impacting the maritime industry and indirectly worldwide shipping industry. Indeed, the decrease in fouling should result in operational costs decrease as much as 161 thousand euros for a single 42 meters long crew vessel. The surface properties of any medical devices play a pivotal role in their functionality. It determines bio-compatibility, reaction to drugs and, most importantly for implants, repulsion or adhesion to living tissue. Titanium implants used today play a major role in orthopedics, as it allows to replace sick or damaged bones.

<b>FEMTO SURF</b>	Document:	Handbook	
	Author:	FEMTIKA	Version: 1
			Date: 29/6/2022

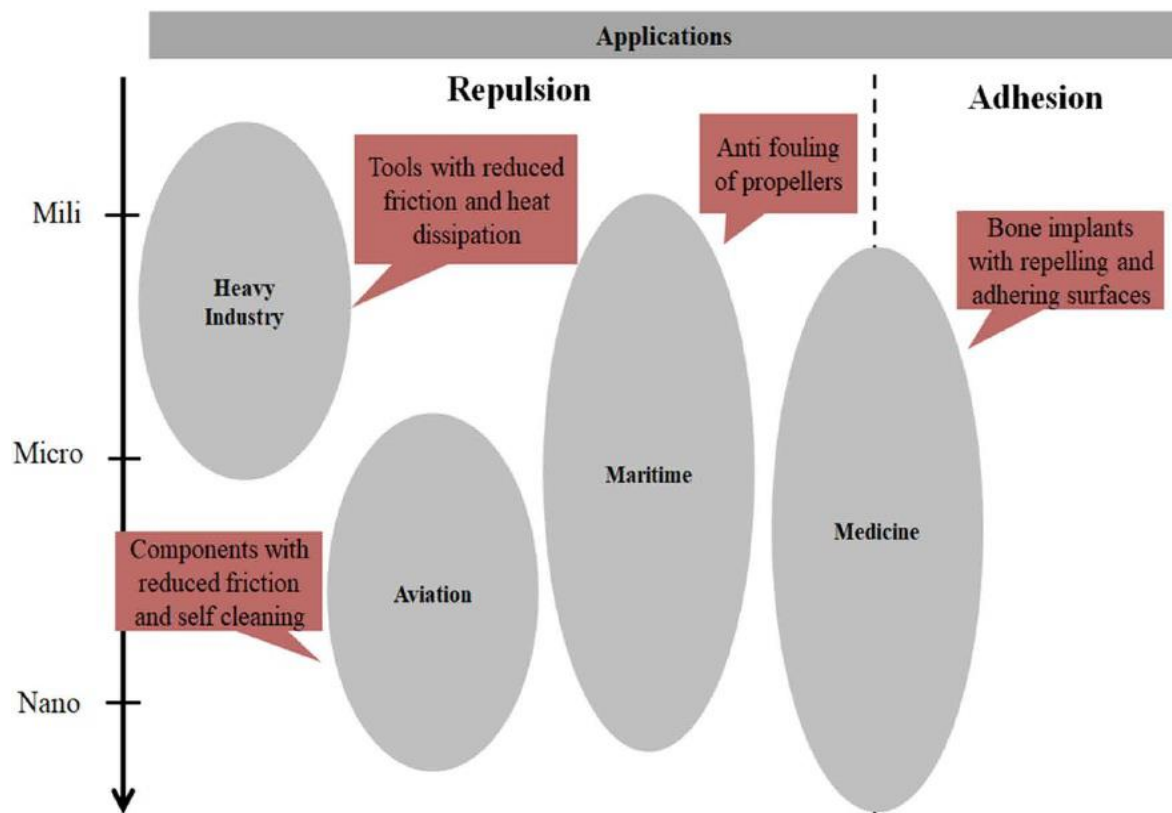



Figure 8. Schematics showing what scale surface features (nano-to-mili) and what properties (repulsion or adhesion) are needed for industries targeted by FemtoSurf.

Thus, well-controlled and spatially targeted repulsion and adhesion properties are a must. At the moment it is achieved with various technologies covering implant in complimentary coatings, that are hard to apply, expensive, prone to wearing and could have long term toxicity, resulting in the necessity to have repeated surgical invasions to the patient's body to reach the implant and treat the long-term wear. FemtoSurf solution would allow to directly tune the properties of titanium implants, including targeted induction of repulsion or adhering in designated areas of the implant. It can be achieved simply by tuning laser and other processing parameters in the setup. Therefore, the FemtoSurf solution will lead to the giant leap forward in the functionality and longevity of orthopedic implants.



	Document:	Handbook		
	Author:	FEMTIKA	Version:	1
			Date:	29/6/2022


## 2 Laser surfaces processing experimentation

### 2.1 Laser parameters effect on materials and alloys, wettability, and topography testing

We began our work by determining the parameters needed to obtain distinct textures such as Dimples, LIPSS, Grooves, and Pillars on each material that could exhibit hydrophobic properties. Such types of textures were selected because they are periodical types and could be differently applied. Parameters were determined purely experimentally. The results are given in Table 1. Interestingly, to acquire a contact angle a greater than  $120^\circ$ , general parameters for all metals proved to be rather similar; this would also allow comparing the same type of texture topography between materials. It is a result of usage of fs pulses, which make processing relatively easy and highly replicable even for different topographies. Both wavelength and pulse duration could be maintained. The repetition rate also could be the same for 3 out of 4 cases - 50 kHz. The only exception was LIPSS, as it benefited from an increased repetition rate. Dimples and LIPSS could also have been fabricated by a higher translation velocity of 0.5 m/s, while grooves and pillars required to reduce it five-fold to 0.1 m/s. However, grooves and pillars could have been made using quite a large scanning spacing - 50 and 60  $\mu\text{m}$ , respectively. Spacing for dimples was also relatively large at 80  $\mu\text{m}$ . LIPSS, on the other hand, needed dense scanning of 4  $\mu\text{m}$ . This can be explained by the fact that dimples, grooves, and pillars are relatively large features made by single non-overlapping scans (laser spot size used with 100 mm F-theta lens - 27  $\mu\text{m}$ ), while LIPSS is a structure that appears at the surface by self-organization. Taking all of this into account, dimples proved to be the slowest surface texture to produce, with a rate of  $0.74 \text{ cm}^2/\text{min}$ , with LIPSS, grooves, and pillars being relatively comparable in terms of manufacturing throughput at  $1.2 \text{ cm}^2/\text{min}$ ,  $2.96 \text{ cm}^2/\text{min}$ , and  $1.8 \text{ cm}^2/\text{min}$ , respectively.

The next question was related to the post-processing of the samples. For it, a direct wettability comparison was made between before and after the second cleaning, shown in Figure 9a. Each sample maintains hydrophilic properties initially, but after cleaning in isopropanol Figure 9b only dimples and LIPSS maintains such properties. After 2 h of heat treatment at  $200^\circ\text{C}$  Figure 9c, most samples again become hydrophobic. Comparing samples between alloys of metals, it seems that on a 17-4PH stainless steel sample fabricated textures after heat treatment show higher hydrophobicity properties than the B sample. In contrast, after heat treatment, only LIPSS textures show hydrophobic properties on the Ti6Al4V sample. Finally, water residue was observed to see if in time wetting properties change under the water drop Figure 9d. Results differed heavily material to material. Only 2024 aluminum samples with dimples and LIPSS had no water residue left. All other samples had some water left on them. It is interesting as initial hydrophobic properties seemed relatively comparable. Therefore, when considering hydrophobic properties, long-term (hours to days) performance needs to be evaluated. After checking the wettability of the textured areas after a substantial amount of time (about 10 month), the wetting properties of hydrophobic textures which were previously observed remained the same. Hydrophilic surfaces, however, became less hydrophilic or even hydrophobic.

*Table 1. Fabrication parameters of each pattern.*

	Document:	Handbook		
	Author:	FEMTIKA	Version:	1
			Date:	29/6/2022

Laser Radiation Parameters	Dimples	LIPSS	Grooves	Pillars
Wavelength	1030 nm			
Pulse duration	500 fs			
Pulse repetition rate	50 kHz	250 kHz	50 kHz	50 kHz
Average power	2 W	1.5 W	5 W	7 W
Fluence	6.99 J/cm <sup>2</sup>	1.05 J/cm <sup>2</sup>	17.47 J/cm <sup>2</sup>	24.45 J/cm <sup>2</sup>
Pulse energy	0.040 mJ	0.0060 mJ	0.10 mJ	0.140 mJ
Pulse per spot	250 pulses	-	-	-
Open shutter time	5 ms	-	-	-
Focusing parameters				
Objective	100 mm F-theta telecentric lens			
Scanning parameters				
Scanning velocity	0.5 m/s	0.5 m/s	0.1 m/s	0.1 m/s
Scanning spacing	80 μm	4 μm	50 μm	60 μm

To understand observed wettability properties and check if they depend on the topography of formed patterns, samples were investigated using an optical microscope. The goal was to see if maybe laser texturing of each metal has any substantial differences in produced patterns. By comparing textures in Figures 10-13 to each sample, it was observed that there are no significant differences between stainless steel alloy dimples, LIPSS, and grooves textures. However, pillar textures proved the most difficult to compare using this methodology but seemed to not yield any significant differences. Furthermore, similar results are obtained between aluminum alloys on each texture. By comparing textures on titanium with other samples' textures, it seems that structures are the most similar to stainless steel. Nevertheless, while there are minimal differences, generally shapes are quite comparable.

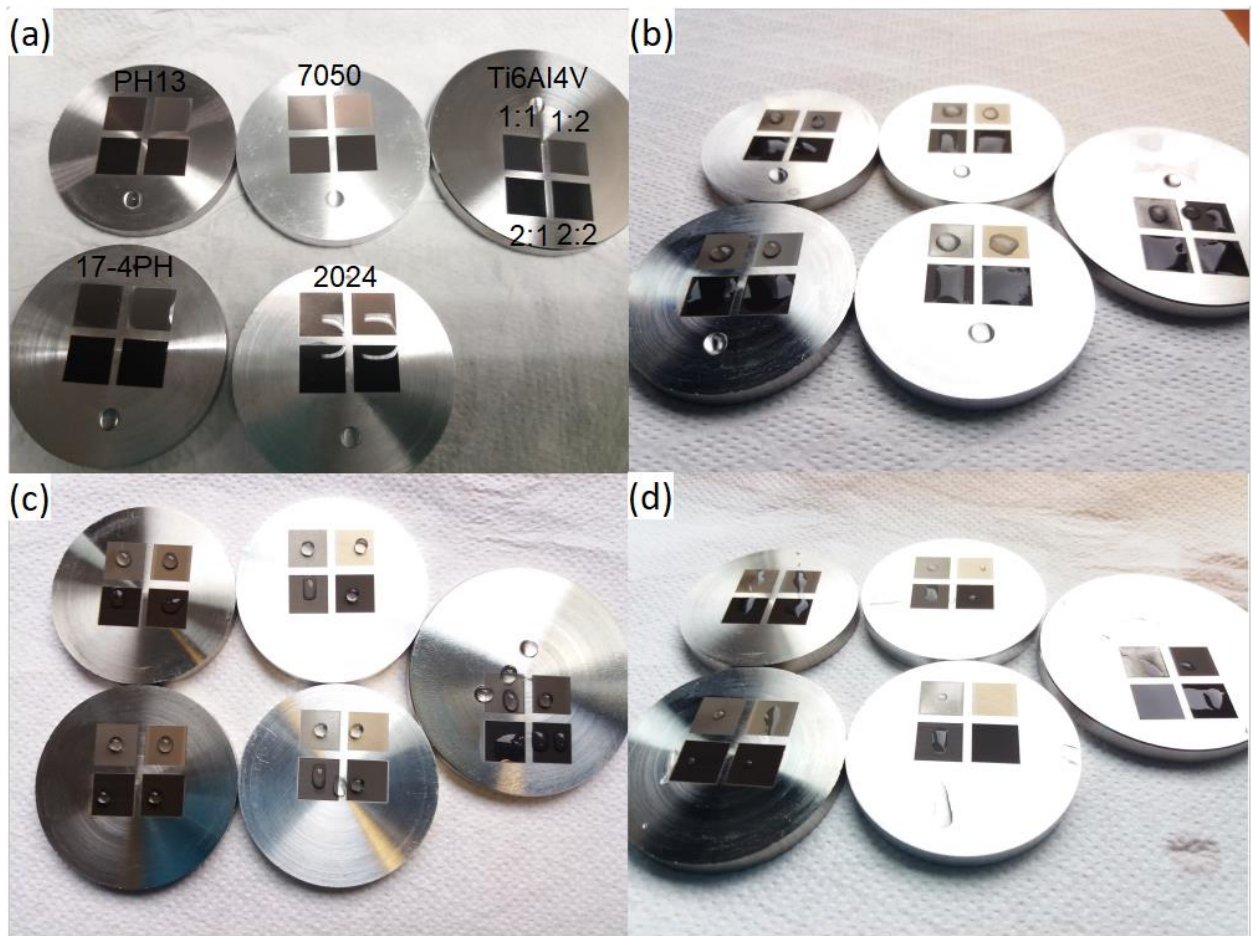



Figure 9. Wettability test of samples. (a)—post fabrication, (b)—post cleaning, (c)—post heat treatment, (d)—water residue. Codes for surface features 1:1—dimples; 1:2—LIPSS; 2:1—grooves; 2:2—pillars. Metals used are labeled in (a).



	Document:	Handbook		
	Author:	FEMTIKA		Version: 1
				Date: 29/6/2022

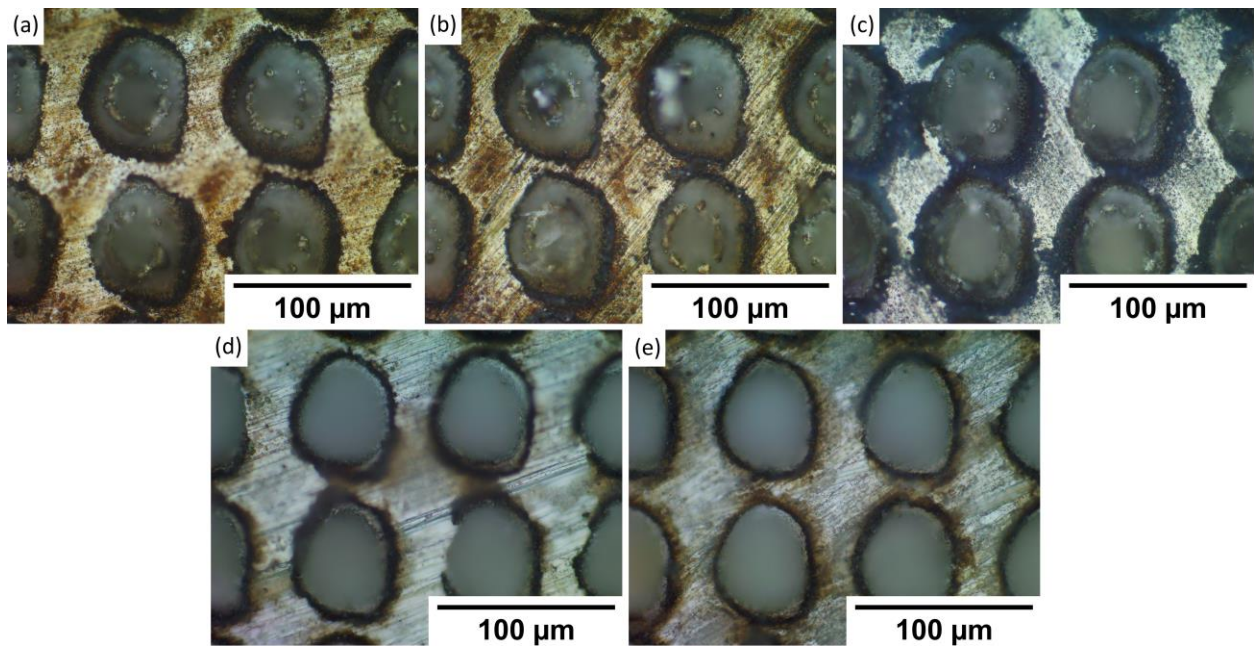


Figure 10. Microscope pictures, with 50x magnification of each sample dimple texture. (a)—17-4PH stainless steel, (b)—PH13 stainless steel, (c)—Ti6Al4V titanium, (d)—2024 T3 aluminum, (e)—7050 aluminum.

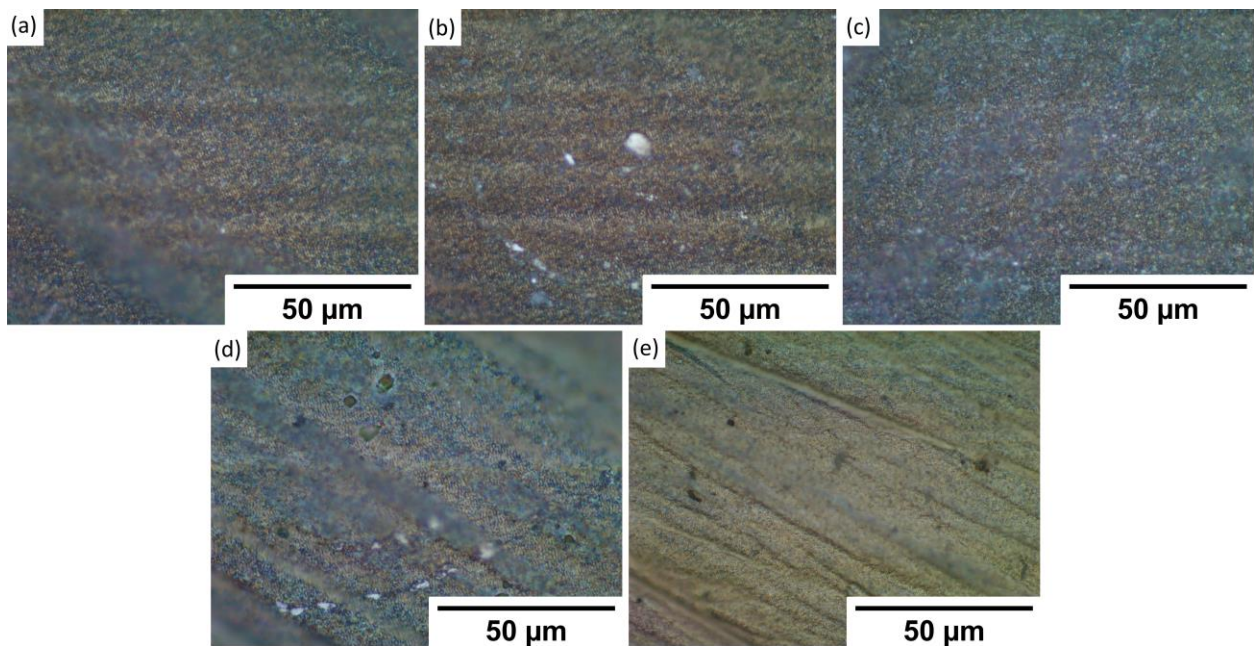



Figure 11. Microscope pictures, with 100x magnification, of each sample LIPSS texture. (a) 17-4PH stainless steel, (b) PH13 stainless steel, (c) Ti6Al4V titanium, (d) 2024 T3 aluminum, and (e) 7050 aluminum.

	Document:	Handbook		
	Author:	FEMTIKA		Version: 1
				Date: 29/6/2022

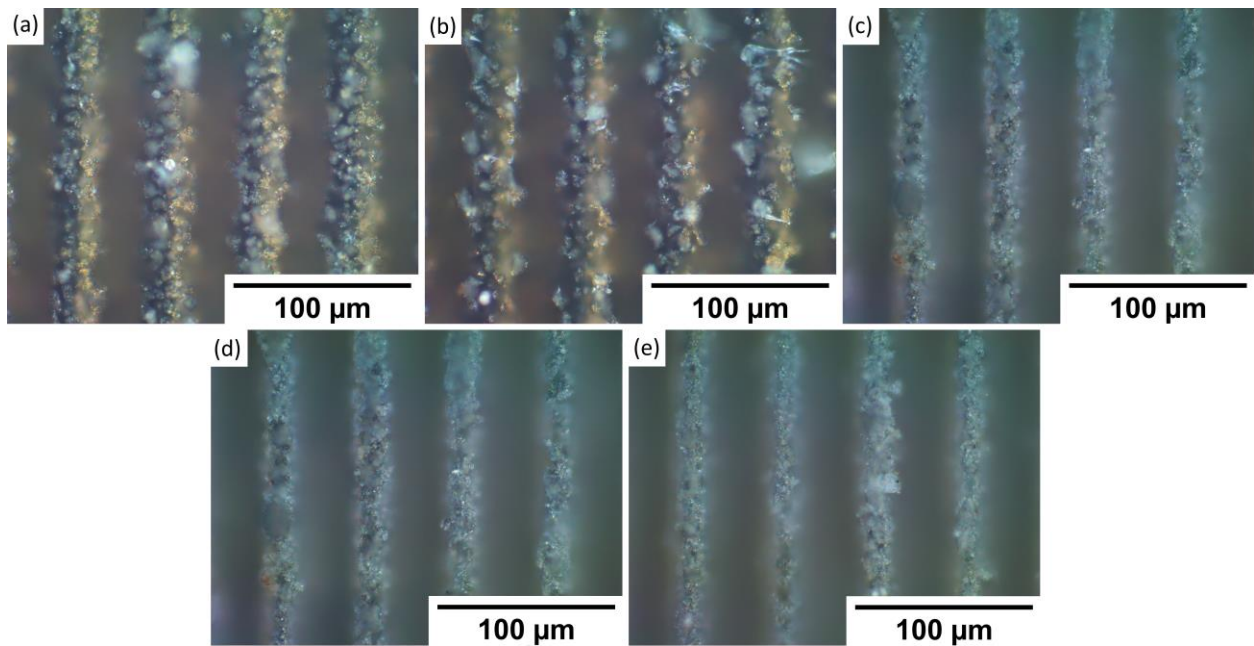


Figure 12. Microscope pictures, with 50x magnification of each sample groove texture. (a) 17- 4PH stainless steel, (b) PH13 stainless steel, (c) Ti6Al4V titanium, (d) 2024 T3 aluminum, and (e) 7050 aluminum.

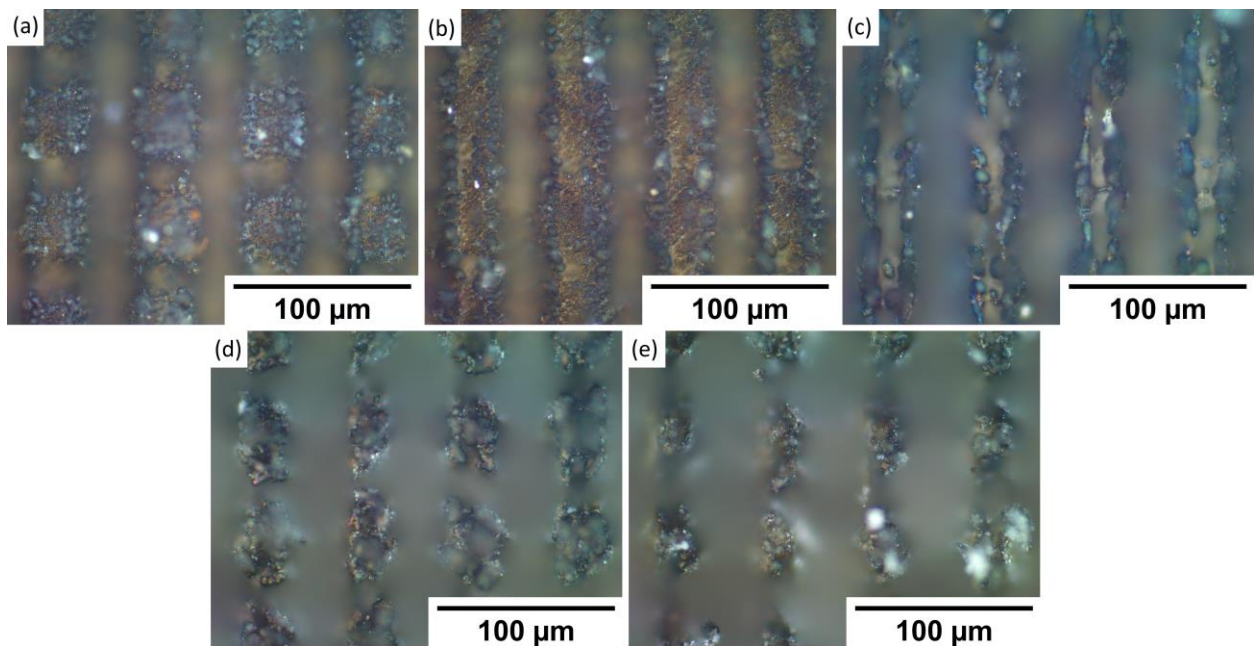



Figure 13. Microscope pictures with 50x magnification of each sample pillar texture. (a) 17-4PH stainless steel, (b) PH13 stainless steel, (c) Ti6Al4V titanium, (d) 2024 T3 aluminum, and (e) 7050 aluminum.



	Document:	Handbook		
	Author:	FEMTIKA	Version:	1
			Date:	29/6/2022

The next step was to compare topography in terms of the profile of formed features in Figures 14 - 17. First, let us compare dimples in Figure 14. Their total depth is in the range from 59  $\mu\text{m}$  for 7-4PH stainless steel to 91  $\mu\text{m}$  with 2024 T3 aluminum. Dimples proved to be the deepest modification compared with LIPPS (which, as expected, were the shallowest), grooves, and pillars. Furthermore, both aluminum samples have dimples that are relatively deeper than steel or titanium. Aluminum samples also have substantially cleaner sides of the profile, while for harder materials some residue material is visible along the sides of the cut. This can be explained by the softer nature of aluminum, allowing easier removal of the material using a laser. A similar trend continued for all the other topographies. Interestingly, a potentially higher degree of residue material left after cutting also resulted in the pillars of PH13 in Figure 17a to be partially transformed back to grooves. However, the overall depth was still significantly different from the grooves of the same material (58  $\mu\text{m}$  grooves vs. 32  $\mu\text{m}$  pillars). Nevertheless, these differences seem to not have a direct correlation with wettability, neither in the short-term, nor long term. Thus, this clearly shows that while general surface topography can help in inducing wettability, it cannot achieve the required result alone.

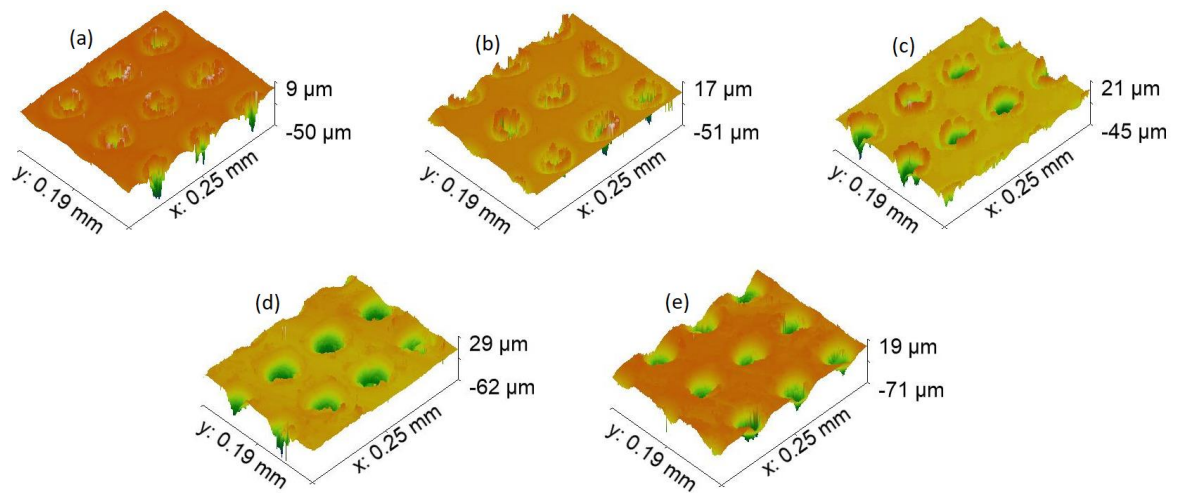



Figure 14. Topography, with 50x magnification of each sample dimple texture. (a) 17-4PH stainless steel, (b) PH13 stainless steel, (c) Ti6Al4V titanium, (d) 2024 T3 aluminum, and (e) 7050 aluminum.

	Document:	Handbook		
	Author:	FEMTIKA		Version: 1
				Date: 29/6/2022

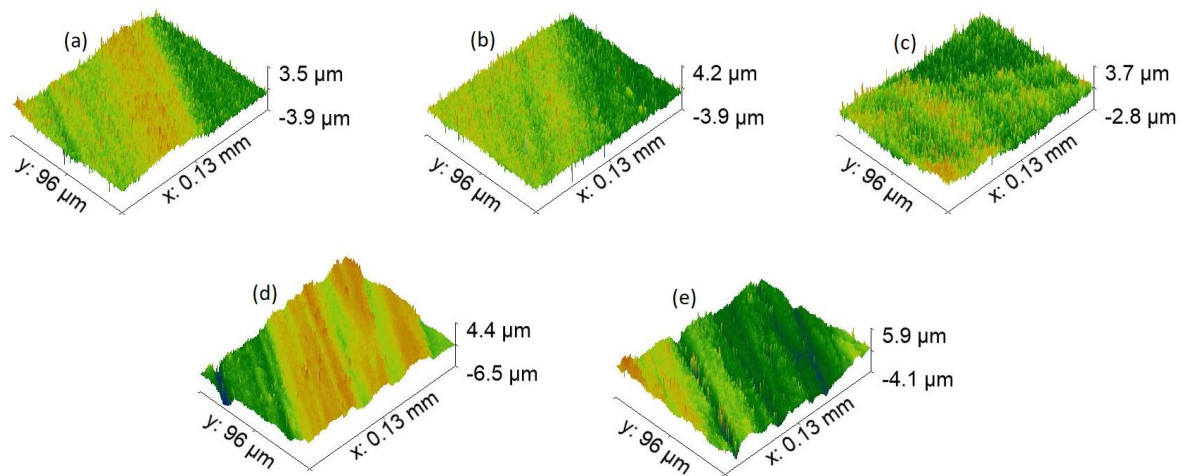


Figure 15. Topography, with 100x magnification of each sample LIPSS texture. (a) 17-4PH stainless steel, (b) PH13 stainless steel, (c) Ti6Al4V titanium, (d) 2024 T3 aluminum, and (e) 7050 aluminum.

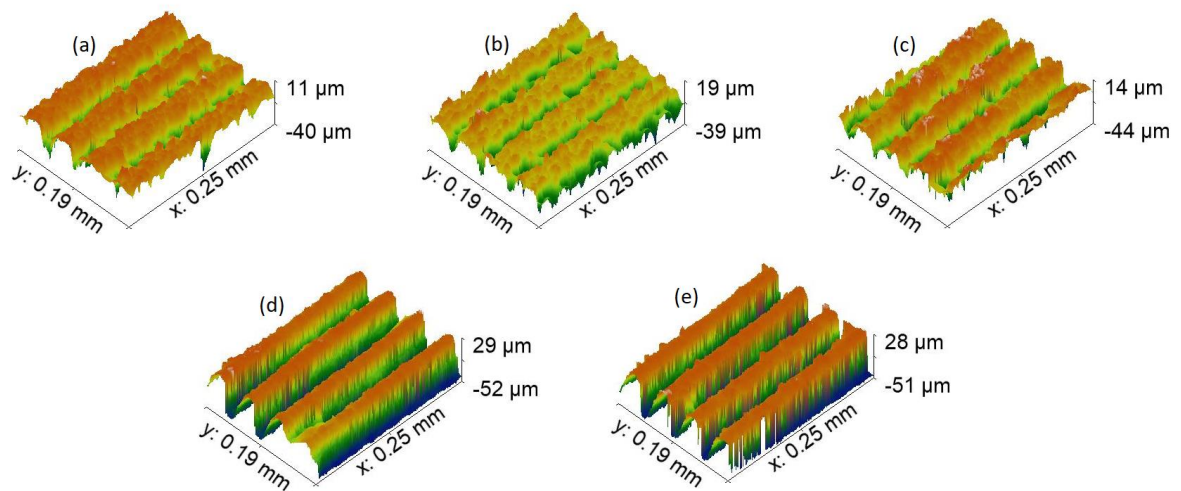



Figure 16. Topography, with 50x magnification of each sample grooves texture. (a) 17-4PH stainless steel, (b) PH13 stainless steel, (c) Ti6Al4V titanium, (d) 2024 T3 aluminum, and (e) 7050 aluminum.

	Document:	Handbook		
	Author:	FEMTIKA		Version: 1
				Date: 29/6/2022

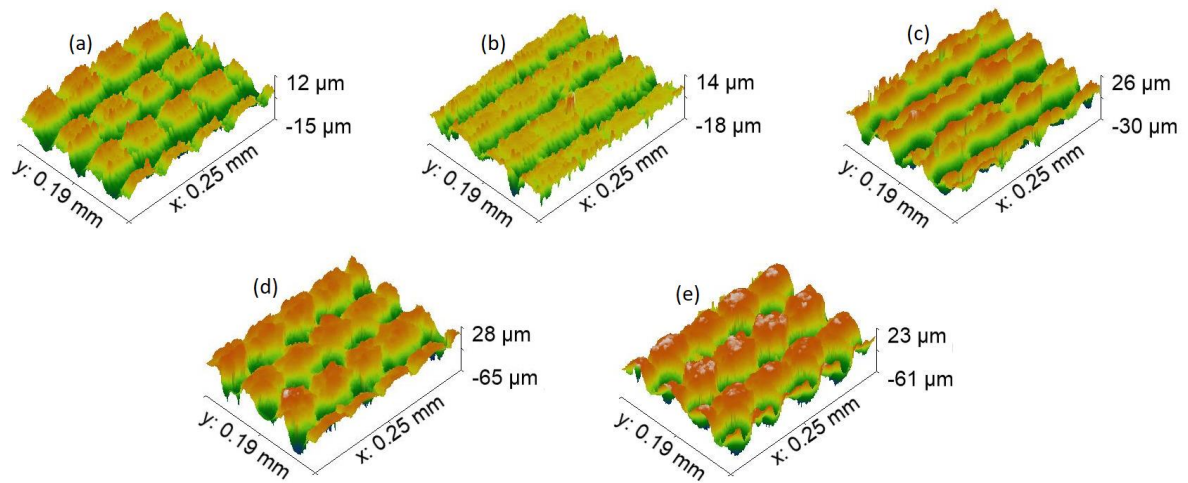



Figure 17. Topography, with 50x magnification of each sample pillars texture. (a) 17-4PH stainless steel, (b) PH13 stainless steel, (c) Ti6Al4V titanium, (d) 2024 T3 aluminum, and (e) 7050 aluminum.

On the other hand, surface chemistry also plays an important role in controlling sample wettability. During heat treatment, the surface starts to oxidize and the amount of -OH groups reduces, forming less active oxides that lower surface energy. At the same time, a small amount of organic and carbon compounds that could be found in air attaches to the surface and forms chemical bonds. This not only decreases surface energy but also surface polarity, so surface wettability shifts to hydrophobicity. So, by looking at chemical composition, heat-treated samples, due to attachment of organic compounds, maintain a higher amount of carbon on the surface, compared with samples right after laser fabrication. It is also possible that attachment of organic, carbon or other compounds could depend on the chemical composition of the material, leading to the formation of different compounds on material and wettability differences. At the same time, there is still a desire to somehow control it and/or induce it on demand.

## 2.2 Heat treatment effect on wettability

Experimentation so far showed that surface features influence wettability, yet it cannot work without proper surface chemistry, while a laser can induce chemical changes via localized heating, it uses up precious laser exposure time. Thus, a much more suitable solution would be to use an auxiliary heat source and post-structuring bake. To prove it, steel and aluminum samples were heated to different temperatures and then induced wettability was measured. Steel and aluminum samples were chosen as these are the most relevant materials for fields of aerospace and shipbuilding. In these areas, contact angle on demand is especially important, as hydrophobic properties can be relevant for anti-icing or anti-fouling, while hydrophilic surfaces might be relevant for better paint adhesion. Results are shown in Figures 18 and 19. Aluminum-produced patterns initially are more hydrophilic. The contact angles of patterns are: dimples - 47°, LIPSS- 6°, grooves - 4°, and pillars - close to 0°. By heating samples in different temperatures, dimple patterns reach 125° contact angle at 205 °C, and in higher temperatures the contact angle starts to decrease. The LIPSS pattern reaches 155° at 175 °C and maintains a similar angle up to 220 °C. From 220 °C to higher temperatures the contact angle starts to decrease. Groove patterns

	Document:	Handbook		
	Author:	FEMTIKA		Version: 1
				Date: 29/6/2022

reach 159° contact angle at 190 °C and maintain a similar angle up to 220 °C. After that, the contact angle starts to decrease in higher temperatures. Pillar pattern reaches 161° contact angle at 205 °C and maintains a similar angle up to 235 °C, after that the temperature contact angle starts to decrease. From all results, it seems that all patterns reach the highest contact angle and maintain it at a temperature between 190 and 220 °C. Furthermore, in higher temperatures all patterns start to decrease. From all tested patterns and obtain results, the highest contact angle provides grooves and pillars, LIPSS provides a slightly lower contact angle, and dimples the lowest. Overall, aluminum offers a lot more tunability using thermal post-treatment.

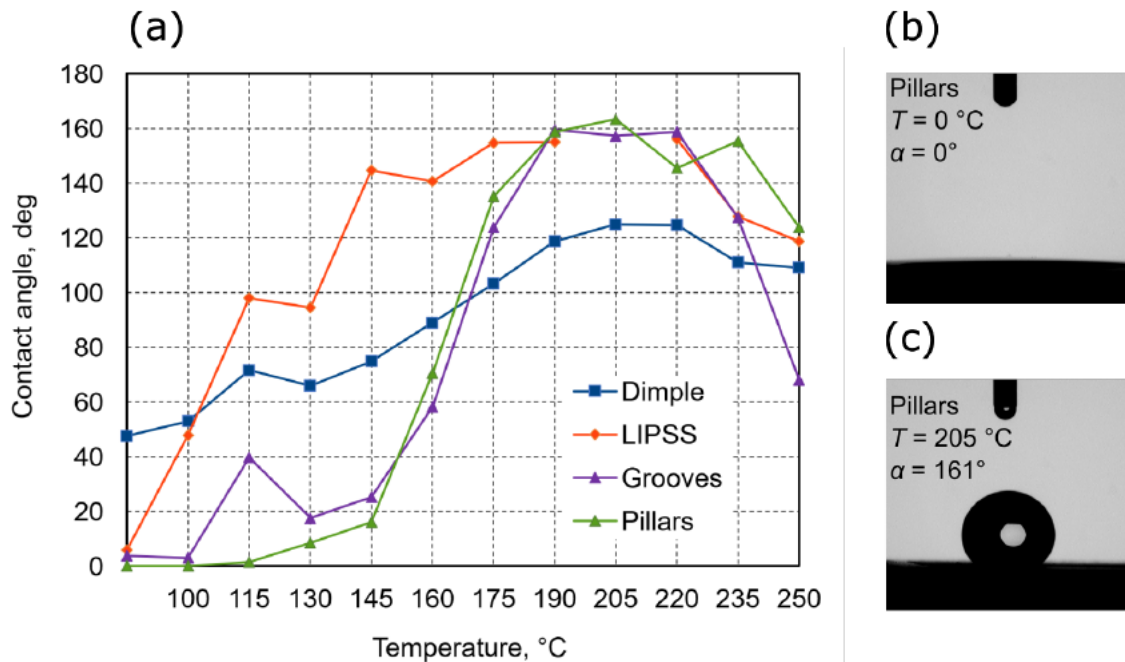


Figure 18. (a) The contact angle of different patterns on aluminum surface dependence heat treatment in different temperatures. (b, c) the lowest and highest acquired contact angle and temperatures needed to induce it.

Same as aluminum, the contact angle of patterns on steel samples were measured. Without heat treatment, patterns on steel are also hydrophilic. Contact angles of patterns are: dimples - 64°, LIPSS - 77°, grooves - 7°, and pillars - 2°. By heating samples in different temperatures, dimple pattern reaches 129° contact angle at 100 °C and then just maintains it in a range between 109 and 131°. LIPSS pattern reaches 143° at 100 °C and then decreases by increased temperature to 101° at 250 °C. The grooves pattern contact angle increased by increasing temperature from 60° at 100 °C and up to 137° at 250 °C. Pillars pattern at 100 °C reaches 128° contact angle and maintains the contact angle from 114° to 141° at 205 °C and then keeps increasing up to 156° at 250 °C. From all the results, it seems that each pattern reacts differently to heat treatment, and contact angles change depending on temperature. The grooves pattern contact angle only increases and possibly could reach even higher in temperatures higher than 250 °C. Pillar's contact angle starts to increase more at 220 °C and could probably increase more in temperatures higher than 250 °C. However, the dimple pattern is quite stable and does not show a high increase or decrease in contact angle depending on temperature. Furthermore, the LIPSS pattern contact angle only decreases in the provided results. It seems that the pillars and grooves patterns show the best hydrophobic properties and could be increased in higher temperatures. Furthermore, LIPSS pattern could

also maintain a higher contact angle if heat treatment were done in lower temperatures. Interestingly, hydrophobicity was achieved almost immediately after heating patterns above 100 °C, showing that it is easy to induce on steel but cannot be tuned much. Furthermore, this experiment proves that patterns play an integral role in contact angle dynamics alongside surface chemistry.

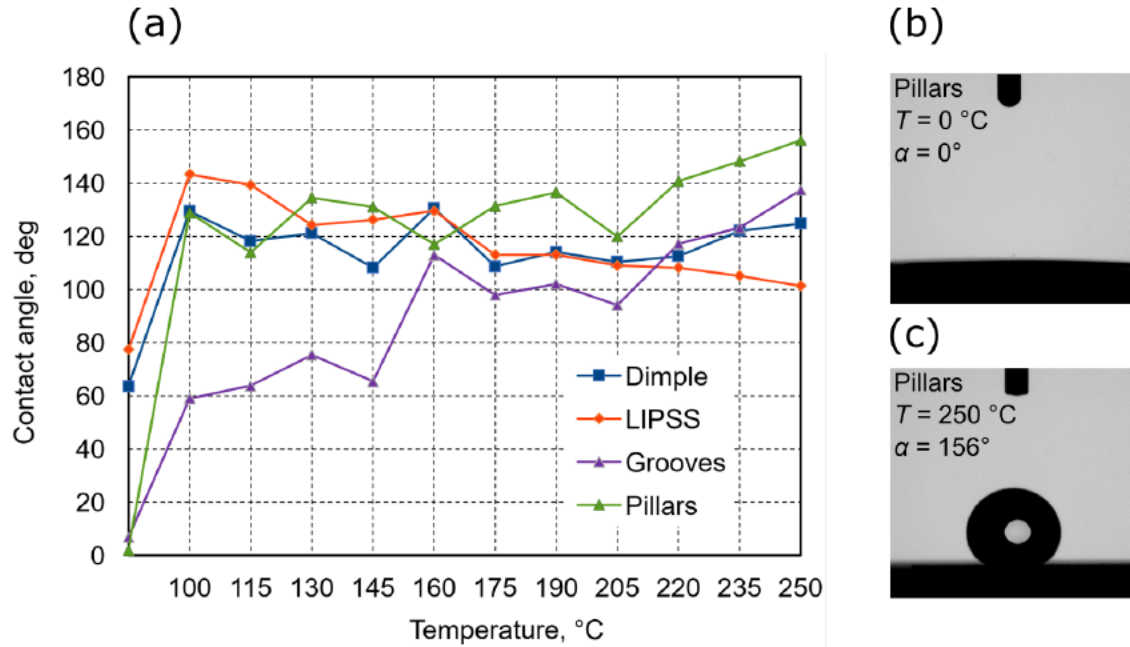



Figure 19. (a) The contact angle of different patterns on steel surface dependence heat treatment in different temperatures. (b, c) the lowest and highest acquired contact angle and temperatures needed to induce it.



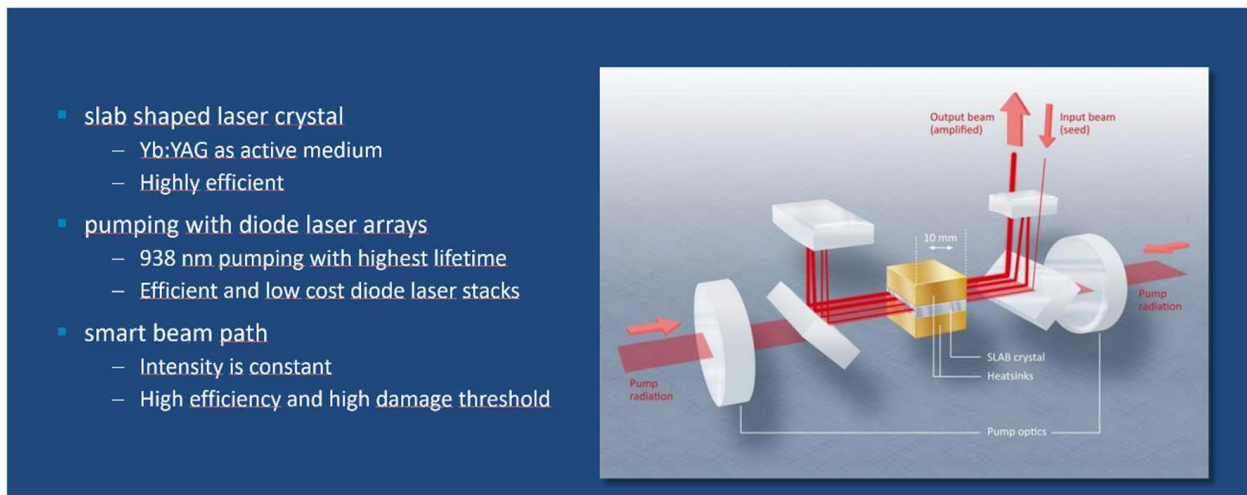
	Document:	Handbook	
	Author:	FEMTIKA	Version: 1
			Date: 29/6/2022

### 3 High power laser development

InnoSlab scheme is shown in picture below. A rectangular shaped laser crystal is pumped with a thin line generated by diode laser stacks. To achieve highly efficient amplification at high output power and high beam quality, a hybrid resonator is used to extract the energy.

#### Yb:InnoSlab Amplification Technology

3 core elements for efficient amplification



The output power can be scaled - maintaining the high beam quality - by increasing the crystal width. This is the focus work within the Femtosurf project. Current systems are using 10 mm wide crystals and achieve an output power of up to 500 W. Based on this, the crystal width for the current InnoSlab amplifier was set to 34 mm with slightly larger crystal length to achieve an output power of >2kW.

#### 3.1 Design of Pumping scheme

The laser crystal is pumped using laser diode bars that are mounted as stacks. In total 24 laser diode arrays are used, which results in a total pump power of 4.8 kW at the 200 W level per array. In the future, laser diodes with up to 300W will be available, the total pump power can be as high as 7.2 kW. Different focusing schemes have been discussed and numerically analyzed. The most promising solution uses a micro-lenses array for homogenization and macroscopic lenses made from special OH-free fused silica glass.




	Document:	Handbook		
	Author:	FEMTIKA		Version: 1
		Date: 29/6/2022		



Figure 20. Lenses that are used for the pumping scheme

The mechanical design of the amplifier units takes into account the optical design of the lenses, the cooling requirements and the alignment strategy of the system. The components for the amplifier have been procured and assembled. A 400 W InnoSlab laser is used as a seed-source for the amplifier. The following graph shows the pump power that has been achieved using the new pumping scheme. Diode lasers are rated up to 220 A. For first experiments they are used up to 180 A. At this current a total output power of 3782 W is focused onto the laser crystal.

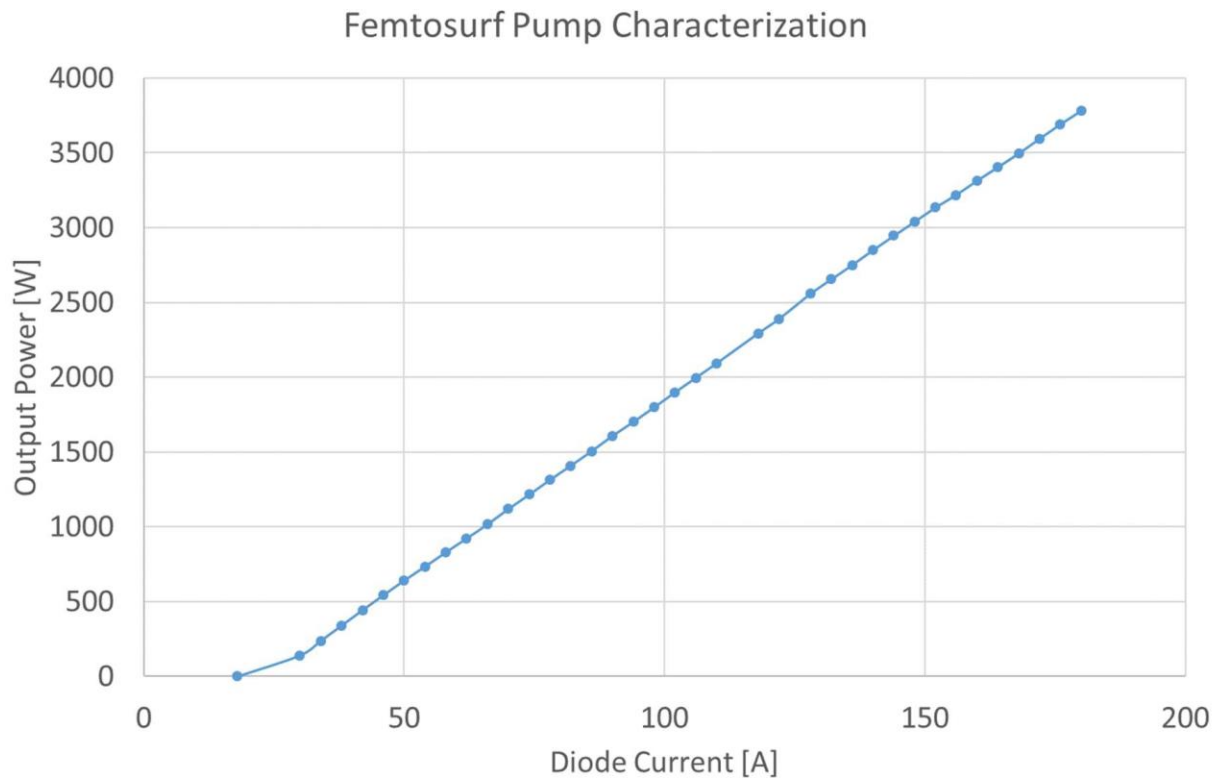

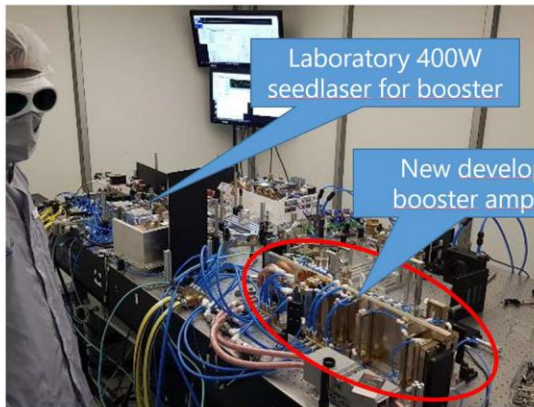


Figure 21. Power characteristics of Pump module at crystal position.

First amplification results have been obtained. A maximum output power after the InnoSlab crystal of 1975 W has been achieved. This is the highest output power reported so far from an InnoSlab type amplifier in the ultrafast pulse duration regime.


	Document:	Handbook		
	Author:	FEMTIKA	Version:	1
			Date:	29/6/2022



Laboratory 400W  
seedlaser for booster

New developed  
booster amplifier

- Optomechanical design of a new booster amplifier based on InnoSlab has been carried out
- All parts have been procured and set up
- First results at 1.975kW output power have been conducted
- The system is running stable. No indication of thermal issues in the new designed pumpsource
- Next step is to investigate the behavior of pump- and Seedlaser parameters

	Document:	Handbook		
	Author:	FEMTIKA		
		Version:	1	
		Date:	29/6/2022	

## 5 FemtoSurf machine

The cantilever solution designed starting from the requirements went through an iterative process of optimization, driving system selection, and components definition to overcome the main identified criticalities. The designed 5-DoF cantilever solution with a 600x600x350 mm working volume. With a positioning accuracy of  $\pm 3 \mu\text{m}$  and a resolution of less than 0.001 mm at maximum speed (25 m/min), the granite-based columnar machine is capable to achieve all set requirements and overcome the current market laser texturing machines. The machine is enriched with all the necessary equipment to allow surface texturing process to be properly performed; the laser-head together with the mirror units and the laser source and its controller as well as the on-board microscopic range vision system.

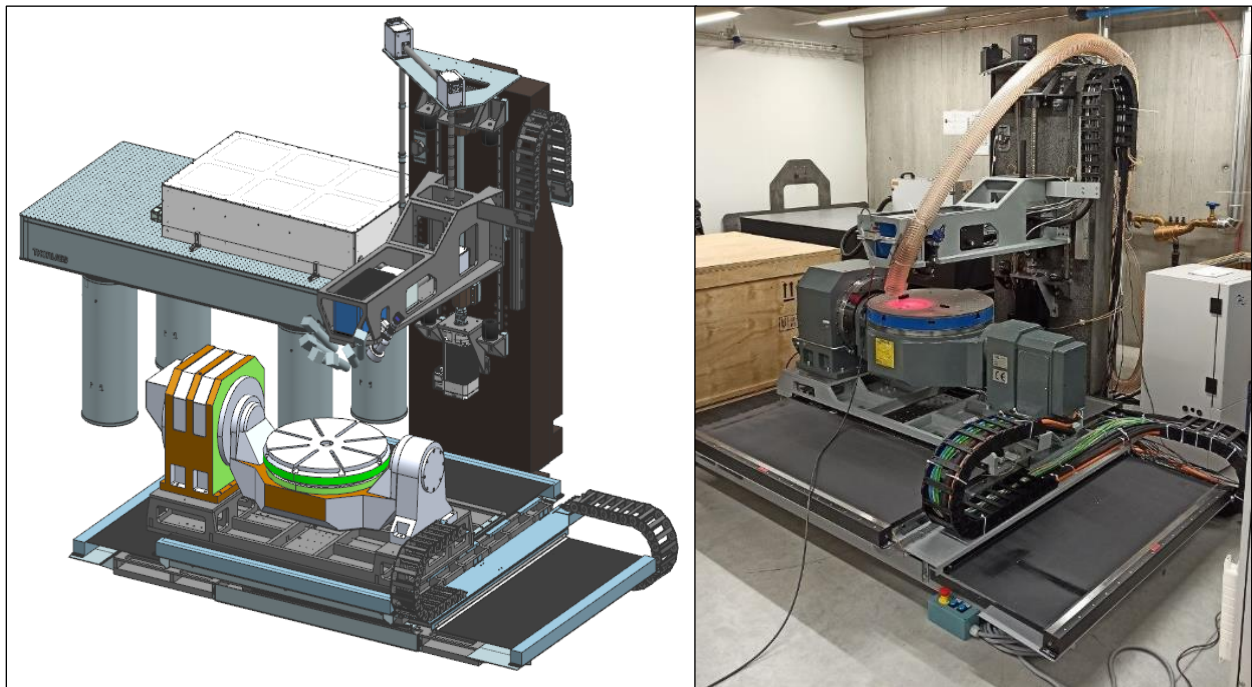

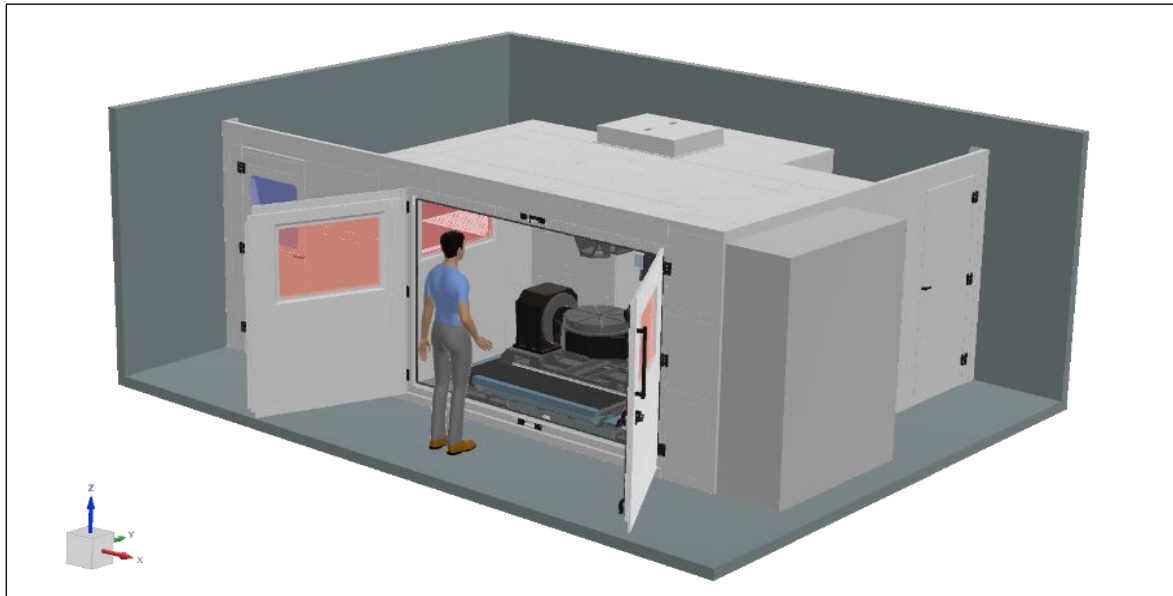


Figure 22. FemtoSurf machine 3D design and final configuration.

An electrical cabinet encloses all the electronic components of the FemtoSurf cell, such as power suppliers, CNC, PLC, motor drives, and safety components. A PC station manages all the machine components with the FemtoSurf SW. In order to maintain the motors and the optics, the laser sources, and the axes motors at a constant desired temperature, two chillers have been installed. The power, the heat to dissipate, and the water flows have been calculated based on the equipment attached to the refrigerator. In order to guarantee reliable functioning of the bearings, linear guides, gears, and screws of the machine a lubricant unit has been implemented, in addition to an oil-based pump system, which controls the machine's brakes.

	Document:	Handbook		
	Author:	FEMTIKA	Version:	1
			Date:	29/6/2022



*Figure 23. 3D CAD model of the external enclosure of the machine.*


The external enclosure allows the operator to closely monitor the process by adopting special laser windows. It is also equipped with a sealed door which ensures the tightness of the chamber. The environmental conditions are created and maintained thanks to a gas management system that will evacuate, filter and cool the polluted gases, which are then reinserted into the enclosure.

The laser beam is deflected along the optical chain with motorized mirrors. A self-alignment closed-loop control has been implemented by Femtika to automatically aligned the beam and avoid process variability due to the laser alignment. The beam entering the mirror black box is partially transmitted on a matrix sensor, which identifies the intensity peak and adjusts the mirror position of the previous black box to have the laser spot centered on the sensor pixel matrix.

Technically speaking, the major challenge faced by the project has been the extension of the Infinite Field of View (IFOV) concept from the state-of-the-art 2D space to the 3rd dimension, to functionalize 3D surfaces like the marine propeller blades of the Rolla use-case. The FemtoSurf control system allows the customization of both the CAD/CAM software algorithms as well as the CNC software to achieve the challenging process requirements. SUPSI has developed three major enhancements:

1. The High Serial Speed Interface (HSSI) communication protocol for the 3D Arges laser scanner, necessary to perform the high-frequency scan head movements and to precisely interpolate the optical axes with the machine's axes.
2. The synchronous triggering of the fs laser source at very specific points along the machine's TCP trajectories, required to generate the micro-treatments on the workpiece surface.



	Document:	Handbook	
	Author:	FEMTIKA	Version: 1
			Date: 29/6/2022

- The implementation in the CNC kernel of the 3rd axis for the 3D IFOV technology, to perform highly precise surface femto laser treatments on 3D surfaces of large workpieces.

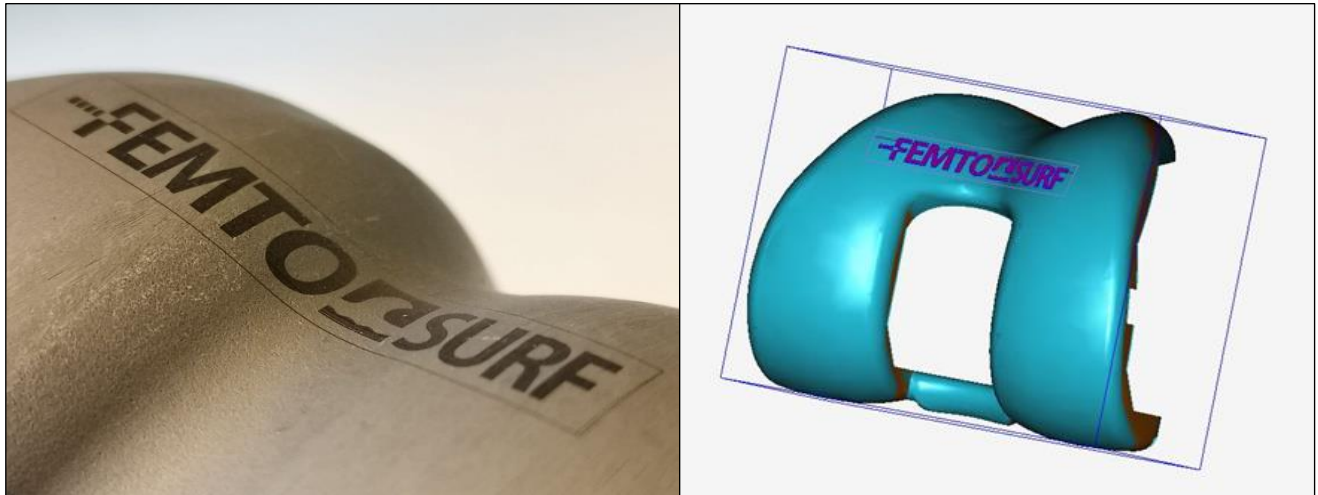


Figure 24. Texturing of the FemtoSurf a Ti64 part, with an irregular surface.

Also in this case it is important to keep the laser beam perpendicular to the surface in each point of the pattern, adapting the position of the part. At the earlier stages of the project, extensive testing on treated surfaces was performed to identify the measurement capability and benefits of the two existing instruments at Heliotis, the H6 and the H8, and their different configurations. While these tests have proven the feasibility to use such a sensor in principle, significant improvements were necessary to deploy the sensor effectively and efficiently, as shown below.

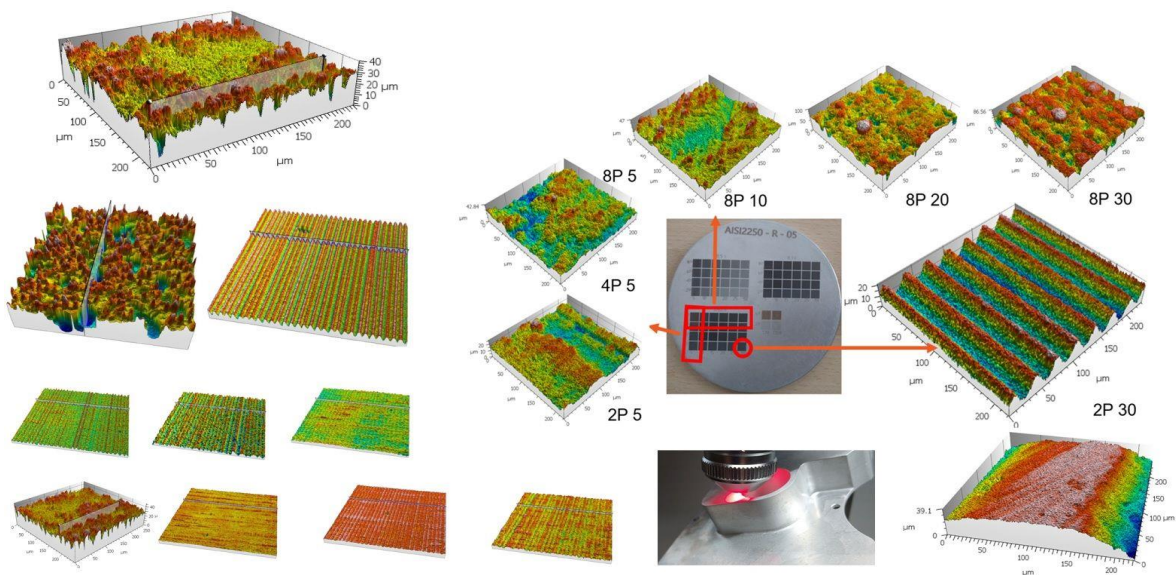



Figure 25. Test measurements.

	Document:	Handbook		
	Author:	FEMTIKA	Version:	1
			Date:	29/6/2022

## 6 Confidentiality

FemtoSurf partners must retain any data, documents, or other material as confidential during the implementation of the project. Further details on confidentiality can be found in Article 36 of the Grant Agreement along with the obligation to protect results in Article 27.